Journal of Alloys and Compounds 509 (2011) 1244–1248

Contents lists available at ScienceDirect

Journal of Alloys and Compounds

journal homepage: www.elsevier.com/locate/jallcom

Effect of Dy on the properties of Sm-doped ceria electrolyte for IT-SOFCs

Yifeng Zheng, Ming Zhou, Lin Ge, Shujun Li, Han Chen, Lucun Guo*

College of Material Science and Engineering, Nanjing University of Technology, No. 5 Xinmofan Road, Nanjing, Jiangsu 210009, PR China

ARTICLE INFO

Article history:
Received 12 August 2010
Received in revised form
29 September 2010
Accepted 30 September 2010
Available online 8 October 2010

Keywords:
Fuel cells
Crystal structure
Ionic conduction
Thermal expansion
SEM
X-ray diffraction

ABSTRACT

Co-doped ceria-based electrolytes of $Ce_{0.8}Sm_{0.2-x}Dy_xO_{2-\delta}$ ($x = 0, 0.02, 0.06, 0.10, 0.14$) were sintered from powders obtained by solid state reaction method. The phase identification, thermal expansion, ionic conductivities and microstructures of samples were studied by X-ray diffraction (XRD), dilatometry, AC impedance spectroscopy (IS) and scanning electron microscopy (SEM). The results showed that the addition of Dy led to higher ionic conductivity and lower activation energy in comparison with Sm singly doped ceria $Ce_{0.8}Sm_{0.2}O_{2-\delta}$ (SDC) in the temperature range of 300–800 °C. As the addition amount of Dy increased up to 2 mol% ($Ce_{0.8}Sm_{0.18}Dy_{0.02}O_{2-\delta}$), the sample attained the highest ionic conductivity, about 50% higher than that of SDC at 500 °C. The effect of Dy on the grain boundary conductivity was more apparent than that of the bulk conductivity. XRD measurements indicated that all the samples were single phase. The thermal expansion was linear for all the samples. The addition of Dy did not change the thermal expansion coefficient (TEC) significantly.

1. Introduction

Confronted with the depletion of fossil fuels, a great deal of efforts has been made to develop and commercialize new energy systems. Solid oxide fuel cells (SOFCs) have attracted increasing interest for their high energy conversion efficiency and pollution-free in generating electricity from hydrocarbons [1–3]. SOFCs based on an yttria stabilized zirconia (YSZ) electrolyte operate at high temperature of 800–1000 °C. Lowering the operation temperature of SOFCs can not only extend the range of material selection, significantly reduce the cost of production and application, but also improve the stability and reliability for SOFCs system. Therefore, there remains a strong motivation to search for new, improved oxide-ion electrolytes at intermediate temperatures (400–800 °C). In recent years, doped ceria has been considered as one of the most promising electrolyte materials for intermediate temperatures SOFCs due to the high ionic conductivity and good compatibility with electrodes [4–7]. Pure cerium oxide is basically not a fast oxygen ion conductor unless it is doped with aliovalent, especially trivalent rare earth ions. The introduction of aliovalent cations into the host lattice can increase the oxygen vacancy concentration and concomitantly improve the ionic conductivity of ceria-based materials [4]. To develop CeO_2-based oxides with improved ionic conductivity, doping of many cations, such as Y, Dy, Gd and Sm, have been investigated extensively, and the highest level of ionic conductivity was reported in Sm-doped compositions [5,8,9]. Moreover, Herle et al. [10] found that co-doping approach showed significantly higher conductivity in air than the best singly doped materials with the same oxygen concentration. Co-doping with rare earth or alkaline earth ion, such as Sm^{3+}, Y^{3+}, La^{3+}, Mg^{2+} or Ca^{2+}, to further improve ionic conductivity has been of interest [11–15]. The ionic radius compatibility of the dopants and the host cation is critical in achieving the right lattice match and thereby the desired properties [4]. However, there is still a lack of systematic studies reported on various ratios of samarium and dysprosium co-doped ceria.

The aim of this study is to investigate the effect of Dy addition on the properties Sm singly doped ceria $Ce_{0.8}Sm_{0.2}O_{2-\delta}$ (SDC). The crystal structure, thermal expansion and ionic conductivity were studied.

2. Experimental

The solid-state compositions of $Ce_{0.8}Sm_{0.2-x}Dy_xO_{2-\delta}$ ($x = 0, 0.02, 0.06, 0.10, 0.14$) were synthesized via a solid-state reaction from CeO_2 (99.5% pure, Yixing Xinwei Leeshing Rare Earth Co., Ltd., China), Sm_2O_3 (99.99% pure, Beijing Founde Star Science and Technology Co., Ltd., China), Dy_2O_3 (99.99% pure, Shanghai Yuelong New Materials Co., Ltd., China) oxides. The powders were weighed according to the stoichiometry milled with zirconia balls in distilled water for 8 h and calcined at 1200 °C for 2 h in air. The as-synthesized powders were milled again for 6 h and dried. The obtained powders were ground and pressed into pellets (13 mm in diameter and 1 mm in thickness) followed by cold-isostatic pressing at about 150 MPa. The green pellets were then sintered at 1600 °C in air for 2 h. Bars of 62 mm × 5 mm × 5 mm were also pressed at 150 MPa for thermal expansion test. The densities of the sintered samples were measured using Archimedean method and were estimated to be 95% of the theoretical density or above.

* Corresponding author. Tel.: +86 25 83587261; fax: +86 25 83306152.
E-mail address: lc-guo@163.com (L. Guo).

0925-8388/$ – see front matter © 2010 Elsevier B.V. All rights reserved.
doi:10.1016/j.jallcom.2010.09.203

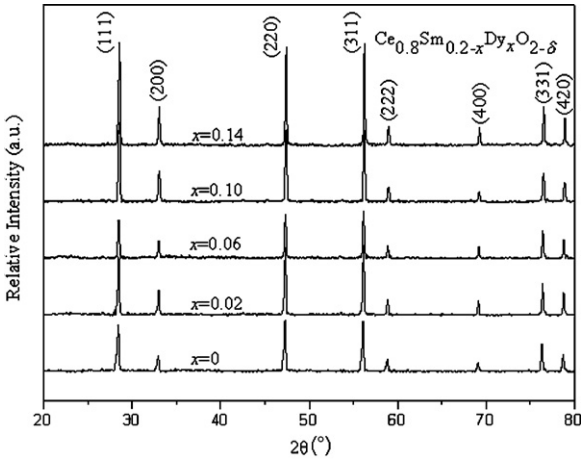

Fig. 1. XRD patterns obtained for $Ce_{0.8}Sm_{0.2-x}Dy_xO_{2-\delta}$ samples after sintering.

The crystal structures of the pellets (ground to powder again for measurement) at room temperature were determined by XRD using the ARL X'TRA diffractometer and Cu Kα radiation. The diffractometer was operated at 40 kV and 35 mA in the scanning range of 20–80°, with the step size of 0.02°. Thermal expansion measurements were conducted with a dilatometer (RPZ-01, Luoyang, China), operated from room temperature to 800 °C in air (heating rate 5 °C/min). The cross-section micrographs of samples were characterized by scanning electron microscopy (SEM, Model Jsm-5900, JEP, Tokyo, Japan). The surfaces were gold-coated to prevent electrostatic charging effect. SEM analysis was carried out at 15 kV accelerating voltage.

In order to prepare samples for the ionic conductivity measurements, silver paste was painted on both sides of the specimens followed by baking at 700 °C for 10 min. The AC impedance spectra of the samples were measured as a function of temperature (300–800 °C) in air using an impedance analyzer (PARSTAT 2273) with the frequency range from 0.1 Hz to 2 MHz. All samples were measured in the same environmental conductions to compare their ionic conductivity values. Curve fitting and resistance calculation were done by ZSimpWin software.

3. Results and discussion

3.1. Phase composition

To ensure the complete dissolution of dopant in CeO_2, XRD patterns were measured for all the doped ceria samples (sintered at 1600 °C for 2 h). Fig. 1 displays the XRD patterns of $Ce_{0.8}Sm_{0.2-x}Dy_xO_{2-\delta}$ samples. The formation of completely phase-pure CeO_2 with cubic fluorite structure (Fm3m) is observed in all the samples. No secondary phases are found in all specimens. It also can be seen that the peaks of $Ce_{0.8}Sm_{0.2-x}Dy_xO_{2-\delta}$ samples shift slightly towards higher angles with Dy content. This is because the ionic radius increases in the order Ce^{4+} (0.97 Å) < Dy^{3+} (1.027 Å) < Sm^{3+} (1.079 Å) [16], so that the increase of Dy content with the decrease of Sm amount in CeO_2 would decrease the magnitude of crystal lattice.

Lattice parameter of each sample was obtained by fitting the peak data of XRD patterns using software Jade. Fig. 2 shows the relationship between lattice parameters and dopant Dy content. It can be seen that the lattice parameters show the linear dependence versus dopant content x, of Dy^{3+} ions. The results in Fig. 2 follow Vegard's rule [17] and further confirm that all the doped ceria samples of this work are ceria-based solid solutions.

3.2. TEC measurements

The electrolyte materials for SOFC must have matched thermal expansion coefficients (TECs) for anode and cathode materials to avoid a microcrack between the anode and electrolyte or between the cathode and electrolyte at the operation temperature. Therefore, thermal expansion is an important property, which governs the performance of high-temperature devices. The exact value

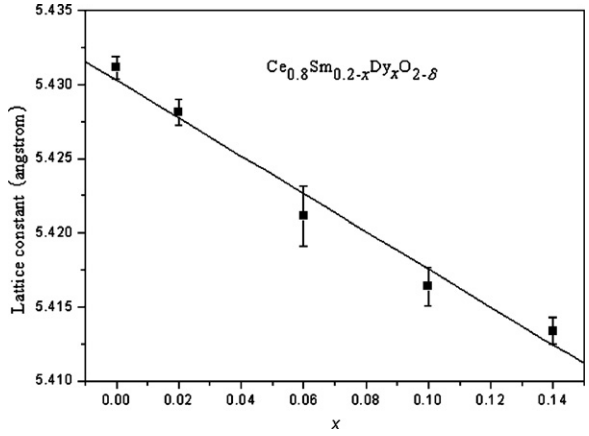

Fig. 2. Lattice parameters of $Ce_{0.8}Sm_{0.2-x}Dy_xO_{2-\delta}$ electrolytes with Dy content (x).

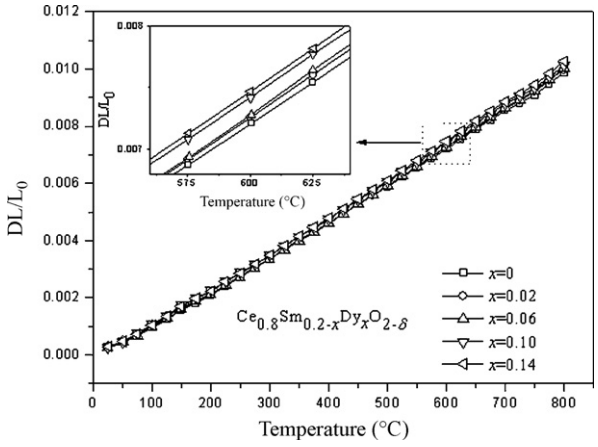

Fig. 3. Linear thermal expansion curves for $Ce_{0.8}Sm_{0.2-x}Dy_xO_{2-\delta}$ in air.

of TEC depends strongly on the composition and the fabrication method of the composition, as well as on the set-up of the thermal expansion measurement.

The thermal expansion characteristic (DL/L_0) of $Ce_{0.8}Sm_{0.2-x}Dy_xO_{2-\delta}$ samples obtained during the heating from 25 to 800 °C in air is shown in Fig. 3, all the samples shows almost change linearly with temperature. In this work, each thermal expansion coefficient (TEC) was calculated from the linear dependence lines during the increase of temperature from 25 to 800 °C, according to the following formula:

$$\alpha_{T_2-T_1} = \frac{DL}{L_0} \times \frac{1}{T_2 - T_1} \quad (1)$$

where $\alpha_{T_2-T_1}$ denotes the average value of TEC in the temperature range of $T_2 - T_1$, L_0 is the initial length of the sample and DL is the change of the sample's length in $T_2 - T_1$.

The TECs of all samples were calculated and listed in Table 1. The TEC value increases slightly with increasing Dy content. According to Kumar et al. [18], the thermal expansion depends on the electrostatic forces within the lattice, which depend on the concentration of positive and negative charges and their distances within the lattice. The thermal expansion increases if the attractive forces decrease. Thus, it was thought that the attractive forces decrease

Table 1
Thermal expansion coefficients of $Ce_{0.8}Sm_{0.2-x}Dy_xO_{2-\delta}$ electrolytes.

$Ce_{0.8}Sm_{0.2-x}Dy_xO_{2-\delta}$	$x=0$	$x=0.02$	$x=0.06$	$x=0.10$	$x=0.14$
TEC ($\times 10^{-6}$ K^{-1})	12.62	12.74	12.77	12.88	13.05

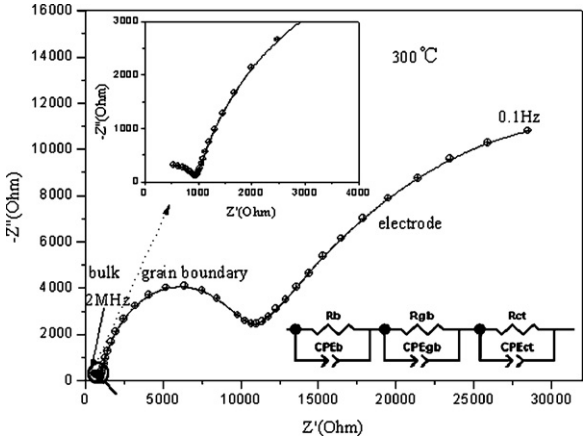

Fig. 4. Impedance spectra obtained for $Ce_{0.8}Sm_{0.14}Dy_{0.06}O_{2-\delta}$ at 300 °C and the equivalent circuit model used for an interpretation of the spectra.

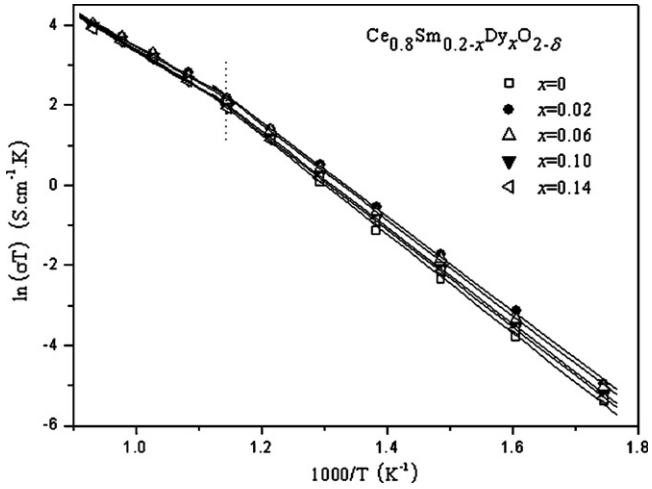

Fig. 5. Arrhenius plots for the total ionic conductivity of $Ce_{0.8}Sm_{0.2-x}Dy_xO_{2-\delta}$.

as a result of the change in lattice parameter (Fig. 2), and that this might yield the increase TEC in the Dy co-doped SDC. The increasing of TEC is accompanied by the decreasing of the lattice parameter. This is in good agreement with the previous reports [18–20]. However, the TECs of Dy co-doped SDC samples only change within 3.5% compared with that of SDC. It indicates that the introduction of Dy into the lattice of SDC does not change the TEC significantly.

3.3. Electrical properties

Fig. 4 shows an exemplary Nyquist impedance spectrum and equivalent circuit model of $Ce_{0.8}Sm_{0.14}Dy_{0.06}O_{2-\delta}$ at 300 °C, at which three separate regions were distinguished. The high frequency part is attributed to the grain interior (bulk) response; the medium frequency semicircle corresponds to grain boundary; and the low frequency arc representing the sample-electrode connection. The contributions of these three parts can be clearly identified in the impedance spectra measured below 500 °C in air in this experiment. The impedance spectra were fitted to the equivalent circuit containing three Resistance-Constant Phase Element (R-CPE) subcircuits in series shown in Fig. 4. These circuits are used only to obtain the best fit and to determine adequately the electrolyte resistance and not to explain the kinetics of redox reactions at the electrodes. At high measurement temperatures (>500 °C), the time constants decrease and the arcs shift to higher frequencies. Therefore, only parts of the arcs appear in the impedance spectrum because of the limited frequency range of equipment. The bulk and grain boundary arcs are associated with the capacitances in the pF and nF ranges, respectively, determined from $2\pi f_{max}RC = 1$, where f_{max} is the applied frequency at arc maximum and R is the arc magnitude [6]. The total resistance of electrolyte is given by:

$$R_t = R_b + R_{gb} \tag{2}$$

where R_b is the bulk resistance and R_{gb} is the grain boundary resistance. Then the total ionic conductivity datum σ at different temperatures can be obtained using the equation:

$$\sigma = \frac{L}{SR_t} \tag{3}$$

where L and S represent the sample thickness and the electrode area of the sample surface, respectively.

The Arrhenius plots for the total ionic conductivity of SDC co-doped with Dy are presented in Fig. 5. It can be seen that the difference in ionic conductivity in the lower temperature region is bigger than that of higher temperature region. This is due to corresponding element valence state and the defect structure trend to be consistent at higher temperature [21]. It can also be noticed that the Arrhenius curve cannot be fitted using a single straight line. The curve should rather be fitted separately by two straight lines, one for the low-temperature range and the other for the high-temperature range. The change of slope is observed at around 600 °C. The similar results were reported earlier by Kim et al. [22]. This indicates that there are differences in conduction mechanism at low (300–600 °C) and at high (600–800 °C) temperatures.

Oxygen ionic conductivity of a solid electrolyte can be described by the following empirical equation:

$$\sigma = \frac{A}{T}\exp\left(-\frac{E}{kT}\right) \tag{4}$$

where E is the activation energy for ionic migration, k is the Boltzman's constant, T is the absolute temperature, and A is the pre-exponential factor being a constant in certain temperature range. For the conduction of rare earth (Dy^{3+}) doped ceria, the total activation energy is the sum of the migration enthalpy (ΔH_m) of oxygen ions and the association enthalpy (ΔH_a) of the complex defects (e.g., $Sm'_{Ce}V''_O/Dy'_{Ce}V''_O$) [23]. The change observed at around 600 °C can be explained by changes in the behaviors of the defects in the $Ce_{0.8}Sm_{0.2-x}Dy_xO_{2-\delta}$ materials [4,24,25]. In the low temperature range (300–600 °C), the oxygen vacancy associated with dopant is trapped as a result of the association of defects to form ($Sm'_{Ce}V''_O/Dy'_{Ce}V''_O$) complexes, so both ΔH_m and ΔH_a influence the conductivity mechanism. As the temperature rises above 600 °C, the oxygen vacancies are free due to the dissociation of these complexes, hence only ΔH_m affects the conductivity mechanism. The enthalpy of all samples is listed in Table 2.

For further comparison, Fig. 6 shows the total ionic conductivity (Fig. 5) which is replotted, with the amount of Dy at two temperatures, one higher (700 °C) and the other lower (500 °C) than 600 °C

Table 2
Enthalpy of $Ce_{0.8}Sm_{0.2-x}Dy_xO_{2-\delta}$ electrolytes.

Parameter		$x=0$	$x=0.02$	$x=0.06$	$x=0.10$	$x=0.14$
$Ce_{0.8}Sm_{0.2-x}Dy_xO_{2-\delta}$	H_m	0.76	0.70	0.72	0.74	0.75
	H_a	0.30	0.32	0.31	0.30	0.29

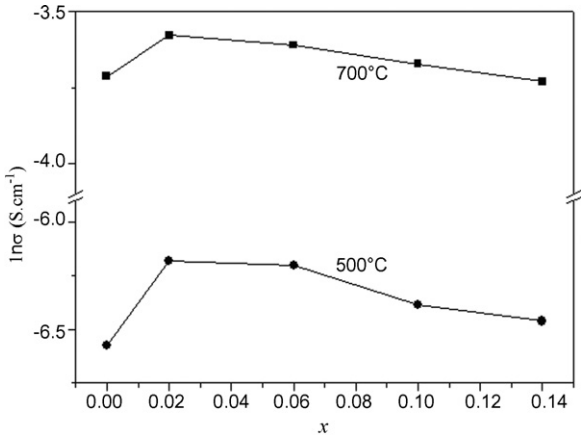

Fig. 6. Variation for the total ionic conductivity of $Ce_{0.8}Sm_{0.2-x}Dy_xO_{2-\delta}$ with Dy content (x) at 500 °C and 700 °C.

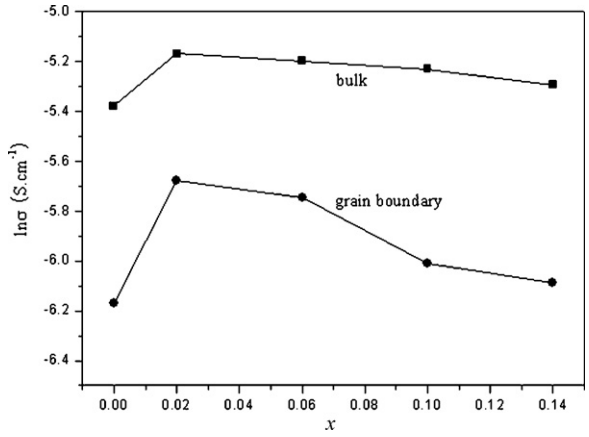

Fig. 8. Bulk and grain boundary conductivity of $Ce_{0.8}Sm_{0.2-x}Dy_xO_{2-\delta}$ with Dy content (x) at 500 °C.

(above mentioned temperature). The variation appears similar at the two temperatures. In comparison with Sm singly doped sample (SDC), the samples of co-doping with appropriate ratio of Sm and Dy show much higher ionic conductivity. This suggests that co-doping effect exists. Dy increases the ionic conductivity of SDC rapidly at $x = 0.02$, and then decrease slightly. At 500 °C, the total ionic conductivity of $Ce_{0.8}Sm_{0.18}Dy_{0.02}O_{2-\delta}$ ($x = 0.02$) is about 50% higher than that of SDC.

The activation energies for total ionic conductivity measured below 600 °C and above 600 °C, obtained from Table 2, are shown in Fig. 7 as a function of composition. As can be seen, the activation energies for conduction of co-doped ceria are lower than that of Sm singly doped ceria, consistent with the results of ionic conductivities shown in Fig. 6. The activation energies for co-doping samples decrease with Dy substitution up to a minimum at $x = 0.02$. The changes of activation energy on composition seem to be correlated with the compositional variations of conductivity—the maximum values of total ionic conductivity corresponds to the minimum activation energy in agreement with the compensation rule of Meyer and Neldel [26].

It has been proved that the ionic conductivity of doped ceria is affected by not only the concentration of oxygen vacancy [11], but also other factors, such as lattice strain [27] and ionic radius [11]. In this study, for the samples of $Ce_{0.8}Sm_{0.2-x}Dy_xO_{2-\delta}$, the partial substitution of Sm with Dy might cause two opposite effects. On the one hand, similar to the results of Yamamura et al. [28], the ordering of the oxygen vacancy might be suppressed, which led to the decrease in activation energy of conduction and the increase in ionic conductivity [5]. On the other hand, the deviation of lattice parameter from host lattice was increased (as shown in Fig. 2), according to results of Kim [29], leading to the increase in activation energy and the decrease in ionic conductivity. Therefore, in order to obtain a desired electrolyte with the higher ionic conductivity and lower activation energy the ratio of Dy to Sm should be well tailored. The optimum addition amount of Dy is about 2 mol% in this study.

Generally, both the bulk and grain boundary contribute to the total ionic conductivity. In this study, the bulk and grain boundary effect for all samples can not be detected above 500 °C because of the effect on the spectra of inductances generated within the experimental apparatus, which is in good agreement with Refs. [4,30]. Therefore, the effect of Dy addition on the bulk and grain boundary conductivity was investigated in the temperature range of 300–500 °C. Fig. 8 shows the bulk and grain boundary conductivity of $Ce_{0.8}Sm_{0.2-x}Dy_xO_{2-\delta}$ at 500 °C. It can be seen that both bulk and grain boundary conductivity are improved by Dy and Sm co-doping, they all reach a maximum at $x = 0.02$. The change of grain boundary is larger than that of bulk with Dy content. It indicates that the effect of the co-doping on the grain boundary conductivity is more apparent than that of the bulk conductivity. Comparing with the magnitude of y-axis for the three curves at 500 °C, the bulk conductivity of samples is much higher than the grain boundary conductivity and total ionic conductivity (Fig. 6). For the samples, the contribution from the grain boundary to the total ionic conductivity dominates so that the overall ionic conductivity is approximately equal to the grain boundary conductivity.

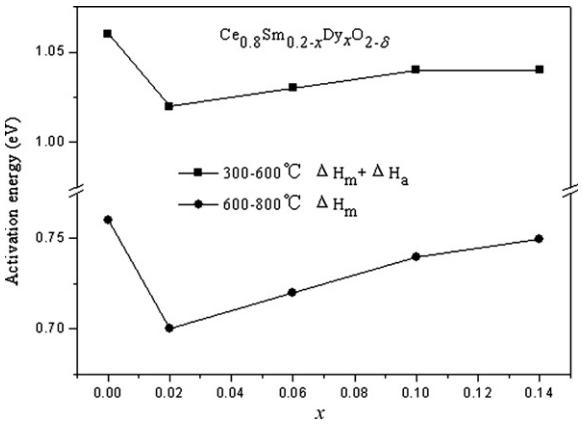

Fig. 7. Activation energy for total ionic conductivity in $Ce_{0.8}Sm_{0.2-x}Dy_xO_{2-\delta}$ measured below 600 °C and above 600 °C, as a function of Dy content (x).

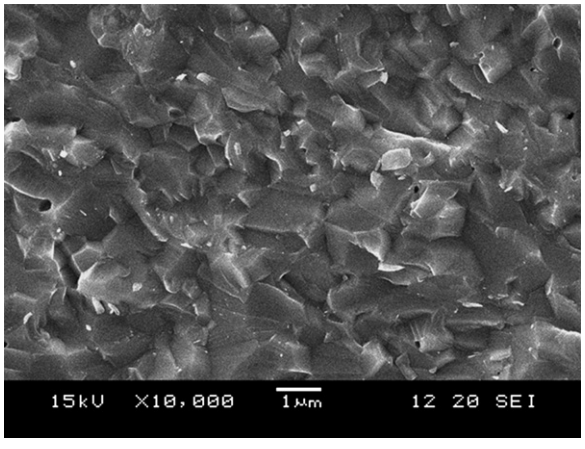

Fig. 9. The cross-section micrograph of $Ce_{0.8}Sm_{0.18}Dy_{0.02}O_{2-\delta}$ sintered pellet.

The microstructure of the sintered pellets of $Ce_{0.8}Sm_{0.2-x}Dy_xO_{2-\delta}$ was studied using SEM. Fig. 9 shows the typical micrograph of the cross-section of $Ce_{0.8}Sm_{0.18}Dy_{0.02}O_{2-\delta}$ sample. All the other doped ceria-sintered samples exhibit similar microstructure as shown in Fig. 9. It can be identified that it is relatively dense except for a few small closed pores, showing a not-fully densified microstructure. It also implies that the ionic conductivity may be further improved by increasing the density.

4. Conclusions

Samples of co-doped ceria with nominal composition of $Ce_{0.8}Sm_{0.2-x}Dy_xO_{2-\delta}$ were prepared and studied. All the sintered samples were fluorite-type ceria-based solid solutions. A linear dependence between the lattice parameter and the content of Dy was observed. The thermal expansion was linear for all the samples. The TEC values of all the compositions were in the range $(12.62–13.05) \times 10^{-6}\,K^{-1}$. In comparison with SDC, the samples of co-doping with appropriate ratio of Sm and Dy showed higher ionic conductivity and lower activation energy in the temperature range from 300 to 800 °C. The bulk and grain boundary conductivity of the samples increased firstly and then decreased with increasing the Dy concentration. The total ionic conductivity was approximately equal to the grain boundary conductivity. In all samples, SDC showed the best improvement in performance when co-doped with 2 mol% Dy.

Acknowledgements

This work was financially supported by the Graduate Science and Technology Innovation Foundation of Jiangsu (CX10B_161Z) and the Science and Technology Pillar Program (Industry) of Jiangsu Province (BE2009169). We also acknowledge the support of Jiangsu Provincial Key Laboratory of Inorganic and Composite Materials.

References

[1] N.Q. Minh, J. Am. Ceram. Soc. 76 (3) (1993) 563–588.
[2] F. Baratto, U.M. Diwekar, J. Power Sources 139 (2005) 188–196.
[3] Y. Matsuzaki, Y. Baba, T. Sakurai, Solid State Ionics 174 (2004) 81–86.
[4] B.C.H. Steele, Solid State Ionics 129 (2000) 95–110.
[5] H. Inaba, H. Tagawa, Solid State Ionics 83 (1996) 1–16.
[6] S. Kuharuangrong, J. Power Sources 171 (2007) 506–510.
[7] E.P. Murray, T. Tsai, S.A. Barnett, Nature 400 (1999) 649–651.
[8] H. Yahiro, K. Eguchi, H. Arai, Solid State Ionics 36 (1989) 71–75.
[9] K. Eguchi, T. Setoguchi, T. Inoue, H. Arai, Solid State Ionics 52 (1992) 165–172.
[10] J.V. Herle, D. Seneviratne, A.J. McEvoy, J. Eur. Ceram. Soc. 19 (1999) 837–841.
[11] T. Mori, J. Drennan, J.H. Lee, J.G. Li, T. Ikegami, Solid State Ionics 154/155 (2002) 461–466.
[12] Y.F. Zheng, H.T. Gu, H. Chen, L. Gao, X.F. Zhu, L.C. Guo, Mater. Res. Bull. 44 (2009) 775–779.
[13] X.Q. Sha, Z. Lu, X.Q. Huang, J.P. Miao, Z.H. Ding, X.S. Xin, W.H. Su, J. Alloys Compd. 428 (2007) 59–64.
[14] F.Y. Wang, S.Y. Chen, Q. Wang, S.X. Yu, S.F. Cheng, Catal. Today 97 (2004) 189–194.
[15] Y.F. Zheng, Y.M. Shi, H.T. Gu, L. Gao, H. Chen, L.C. Guo, Mater. Res. Bull. 44 (2009) 1717–1721.
[16] R.D. Shannon, Acta Crystallogr. A 32 (1976) 751–767.
[17] M. Mogensen, N.M. Sammes, G.A. Tompsett, Solid State Ionics 129 (2000) 63–94.
[18] V.P. Kumar, Y.S. Reddy, P. Kistaiah, G. Prasad, C.V. Reddy, Mater. Chem. Phys. 112 (2008) 711–718.
[19] G.C. Kostogloudis, N. Vasilakos, C. Ftikos, Solid State Ionics 106 (1998) 207–218.
[20] G.C. Kostogloudis, C. Ftikos, Solid State Ionics 135 (2000) 537–541.
[21] X.Q. Sha, Z. Lu, X.Q. Huang, J.P. Miao, L. Jia, J. Alloys Compd. 424 (2006) 315–321.
[22] N. Kim, B.H. Kim, D. Lee, J. Power Sources 90 (2000) 139–143.
[23] T.S. Zhang, J. Ma, L.B. Kong, S.H. Chan, J.A. Kilner, Solid State Ionics 170 (2004) 209–217.
[24] R.O. Fuentes, R.T. Baker, J. Power Sources 186 (2009) 268–277.
[25] Y.B. Go, A.J. Jacobson, Chem. Mater. 19 (2007) 4702–4709.
[26] W. Meyer, H. Neldel, Z. Tech. Phys. 12 (1937) 588–593.
[27] X.F. Guan, H.P. Zhou, Z.H. Liu, Y.N. Wang, J. Zhang, Mater. Res. Bull. 43 (2008) 1046–1054.
[28] H. Yamamura, E. Katoh, M. Ichikawa, K. Kakinuma, T. Mori, H. Haneda, Electrochemistry 68 (2000) 455–459.
[29] D.J. Kim, J. Am. Ceram. Soc. 72 (1989) 1415–1421.
[30] R.O. Fuentes, R.T. Baker, Int. J. Hydrogen Energy 33 (2008) 3480–3484.